Sound Velocity Measurements of B2-Fe-Ni-Si Alloy Under High Pressure by Inelastic X-Ray Scattering: Implications for the Composition of Earth's Core

HPSTAR
1501-2022

S. Dominijanni[1] , C. A. McCammon[1] , E. Ohtani[2] , D. Ikuta[2] , T. Sakamaki[2], T. Ishii[3], G. Criniti[1] , L. S. Dubrovinsky[1], S. Khandarkhaeva[1], T. Fedotenko[4], K. Glazyrin[4] , H. Uchiyama[5] , H. Fukui[5] , and A. Q. R. Baron[5,6]

[1]Bayerisches Geoinstitut, University of Bayreuth, Bayreuth, Germany, [2]Department of Earth and Planetary Materials Science, Graduate School of Science, Tohoku University, Sendai, Japan, [3]Center for High Pressure Science and Technology Advanced Research, Beijing, China, [4]Photon Science, Deutsches Elektronen Synchrotron, Hamburg, Germany, [5]Japan Synchrotron Radiation Research Institute, Sayo-gun, Japan, [6]Materials Dynamics Laboratory, RIKEN SPring-8 Center, Sayo-gun, Japan

Abstract Elastic properties of B2-$Fe_{0.67}Ni_{0.06}Si_{0.27}$ (15 wt.% Si) alloy have been investigated by combined high-resolution inelastic X-ray scattering and powder X-ray diffraction in diamond anvil cells up to 100 GPa at room temperature. Densities (ρ), compressional (V_P) and shear (V_S) wave velocities were extrapolated to inner core conditions to enable comparison with the preliminary reference Earth model. The modeled aggregate compressional and shear wave velocities and densities of the two-phase mixture of B2-$Fe_{0.67}Ni_{0.06}Si_{0.27}$ and *hcp*-Fe-Ni are consistent with inner core PREM values of V_P, V_S, and ρ based on a linear mixing model with 30(5) vol % B2-$Fe_{0.67}Ni_{0.06}Si_{0.27}$ and 70(5) vol % *hcp* Fe-Ni, which corresponds to ∼3–5 wt.% Si and ∼5–12 wt.% Ni.

Plain Language Summary The composition of the inner core holds key information about how Earth evolved and how current processes such as the geomagnetic field work. Because the core cannot be directly sampled, our best estimates of its composition are based on the comparison of geophysical data with laboratory measurements of candidate materials. Decades of study have shown the inner core to be composed mainly of iron (with a minor amount of nickel) alloyed with one or more light elements, such as silicon. However, the effect of Si on the geophysical properties of Fe-Ni alloys is not well established. In this study, we performed laboratory experiments to determine the density and sound velocity of Fe-Ni-Si alloy under extreme pressure conditions. We compared our results with seismological determinations and found that Earth's inner core can be accounted for by a mechanical mixture of cubic Fe-Ni-Si and hexagonal Fe-Ni alloys. This mixture has a bulk composition of ∼3–5 weight % Si and ∼5–12 weight % Ni and is consistent with geophysical constraints.

1. Introduction

Our knowledge of the structure and composition of Earth's core is based on sparse direct evidence (e.g., from seismology, geodesy, geo- and paleo-magnetism) and many indirect observations (from cosmochemistry, experimental petrology, and mineral physics) (Allègre et al., 1995; McDonough & Sun, 1995). Cosmochemical studies on iron meteorites and a comparison of mineral physics data with seismological observations (measurements of density (ρ) and compressional (V_P) and shear (V_S) wave velocities under extreme conditions) suggest that Earth's inner core is primarily composed of metallic Fe-Ni alloy (5-25 wt.% Ni) (McDonough & Sun, 1995; Wasson & Chou, 1974). However, the inner core density is ∼5 % lower than pure Fe at corresponding pressures and temperatures (Dewaele et al., 2006; Fei et al., 2016), presumably due to the presence of light elements (Birch, 1952) that were incorporated in the core during its formation (Rubie et al., 2011; Siebert et al., 2013; Wade & Wood, 2005). Oxygen, silicon, sulfur, carbon, and hydrogen have been proposed as candidates based on geochemical and geophysical evidence (Birch, 1964; H. K. Mao et al., 1990). Si is favored based on its effect on the compressional wave velocities of iron (Antonangeli et al., 2010; Badro et al., 2007; Lin et al., 2003; Z. Mao et al., 2012) and its affinity for the metallic phase during Earth's differentiation (Fischer et al., 2015 ; Siebert et al., 2013; Tateno et al., 2015).

Phase relations and *P-V-T* equations of state have been investigated for various compositions in the Fe-Si (Asanuma et al., 2008; Dobson et al., 2002, 2003; Edmund, Antonangeli, Decremps, Morard, et al., 2019; Edmund, Antonangeli, Decremps, Miozzi, et al., 2019; Fischer et al., 2012, 2013; Hirao et al., 2004; Kuwayama et al., 2009; Lord et al., 2010; Lin et al., 2009; Zhang & Guyot, 1999a, 1999b) and Fe-Ni-Si (Edmund et al., 2020; Ikuta et al., 2021; Morrison et al., 2018; Sakai et al., 2011) systems. Stoichiometric FeSi is stable in the B20 (FeSi-type) structure under ambient conditions (Fischer et al., 2013). With increasing pressure and temperature, a B20 + B2 (CsCl-type) mixture becomes stable at least up to ∼40 GPa (Caracas & Wentzcovitch, 2004; Dobson et al., 2002, 2003; Fischer et al., 2013; Lord et al., 2010; Vočadlo et al., 1999), where it transforms to the B2 structure that persists up to 145 GPa (Fischer et al., 2013). Variation of the Si content in the Fe-FeSi system promotes the stability of the *hcp* structure at high pressure (Fischer et al., 2013). The coexistence of B2 + *hcp* phases was observed up to 145 GPa and 2400 K for a Fe-Si alloy with Si content ranging from 9 to 16 wt.% (Fischer et al., 2013). Extrapolation of the *hcp* + B2 phase boundaries at 329 GPa and 6650 K indicates that Si-bearing Fe alloys could be stable as a mechanical mixture of Si-depleted (Si < 2 wt.%) *hcp* and Si-enriched (Si > 10-15 wt.%) B2 phases at Earth's inner core conditions (Fischer & Campbell, 2015; Fischer et al., 2012, 2013). The presence of this two-phase mixture at inner core conditions is also supported by X-ray studies in the Fe-Ni-Si system (Ikuta et al., 2021).

Traditionally, the core composition has been inferred from sound velocity measurements compared with the preliminary reference Earth model (PREM, Dziewonski & Anderson, 1981) based on an inner core consisting of a single phase. Sound velocity studies include inelastic X-ray scattering (IXS): Fe (H. K. Mao et al., 2001); Fe-Si (Antonangeli et al., 2010); FeH_x (Shibazaki et al., 2012); Fe (Ohtani et al., 2013); Fe (Liu et al., 2014); Fe (Sakamaki et al., 2016); Fe-Si (Antonangeli et al., 2018); Fe-Si (Sakairi et al., 2018), nuclear resonance inelastic X-ray scattering (NRIXS): Fe-Si (Lin et al., 2003), ultrasonic: Fe (Shibazaki et al., 2016), shock wave: for example, Fe-Si (Brown & McQueen, 1986), and Picosecond Acoustics (PA) experiments: Fe-Si (Edmund, Antonangeli, Decremps, Morard, et al., 2019; Edmund, Antonangeli, Decremps, Miozzi, et al., 2019). Inferences of inner core composition vary. Using IXS, Badro et al. (2007) and Antonangeli et al. (2010, 2018) concluded that a Fe-Si alloy with about 2 wt.% Si could account for geophysical observations of the inner core. Conversely, Z. Mao et al. (2012) and Sakairi et al. (2018) proposed higher silicon contents, 8 wt.% and 3-6 wt.% Si, respectively, to match seismological observations. The highest estimate indicates a Si content up to ∼20 wt.% in Earth's core (Balchan & Cowan, 1966; Ringwood, 1959). Recent measurements performed using the PA technique (Edmund, Antonangeli, Decremps, Morard, et al., 2019) report that Fe alloy containing 5 wt.% Si matches PREM inner core density but does not account for geophysically observed compressional and shear wave velocities.

In the present study, we take a different approach and test the hypothesis that the inner core is composed of a mixture of Si-depleted *hcp* and Si-enriched B2 phases. In previous studies, X-ray diffraction (XRD) data combined with sound velocities taken from the literature supported this speculation (Fischer et al., 2015; Ikuta et al., 2021), but involved many assumptions regarding sound velocities. Our work provides the first test of the hypothesis through direct high-pressure measurements of the sound velocities and density of polycrystalline B2-$Fe_{0.67}Ni_{0.06}Si_{0.27}$ using IXS and powder XRD.

2. Materials and Methods

2.1. Sample Synthesis

The starting material was made from powders of reagent-grade metallic Fe (99.9% purity), Ni (99.7% purity), and Si (99.9995% purity). We mechanically ground the mixture of Fe (78 wt.%), Si (15 wt.%), and Ni (7 wt.%) for about 1 hr in an agate mortar under ethanol to achieve a homogeneous mixture.

Two different samples (runs H4973 and S7389) of Fe-Ni-Si alloy were synthesized using the 1,000-ton and 1,200-ton Kawai-type multi-anvil apparatus at Bayerisches Geoinstitut, University of Bayreuth (BGI). Multi-anvil experiments were carried out using tungsten-carbide cubes with truncation edge lengths of 11 mm. A Cr_2O_3-doped MgO octahedron with an edge length of 18 mm (18/11 configuration) was used as a pressure medium. A triple-stepped graphite heater was used to reduce the thermal gradient inside the capsule (Rubie, 1999). Thermal insulation was provided by a ZrO_2 sleeve located outside the heater. A single crystal MgO capsule loaded with the starting mixture was placed inside the cylindrical heater. A thin polycrystalline MgO sleeve was placed between the capsule and the heater. Sample temperature was monitored using a $W_{97\%}Re_{3\%}$–

$W_{75\%}Re_{25\%}$ (D-type) thermocouple directly in contact with the top of the MgO capsule. Synthesis experiments were performed at sub-solidus conditions at 8.0(5) GPa and 1200(50) °C, where uncertainties are estimated according to Rubie (1999). After 1 hr, during which temperature was maintained within ±10–20 °C, experiments were quenched rapidly by switching off the power and then decompressed to ambient pressure over 15 hr.

Recovered MgO capsules were mounted in epoxy and polished to expose the samples for phase identification and compositional analysis. Phase identification of H4973 and S7389 samples were made using the microfocus X-ray powder diffractometer (MF-XRD) Bruker D8 DISCOVER (Co-Kα wavelength of 1.78 Å) installed at BGI. Results showed only *fcc* Fe-Ni-Si (Figure S1 in Supporting Information S1). Sample homogeneity was confirmed using a scanning electron microscope (SEM, ZEISS LEO 1530) with an energy dispersive X-ray spectrometer. SiO_2, Fe, and Ni were used as standards for chemical analyses. Alloy compositions were calculated to be $Fe_{0.665(2)}Ni_{0.060(1)}Si_{0.275(5)}$ and $Fe_{0.666(2)}Ni_{0.060(1)}Si_{0.274(1)}$ for H4973 and S7389, respectively. Examples of backscattered electron (BSE) images are given in Figures S2a and S2b in Supporting Information S1, which show polycrystalline textures with grain sizes ranging from ∼5 to 20 μm.

2.2. Diamond Anvil Cell Experiments

A fragment of the alloy was placed inside a drilled Re gasket hole that was pre-indented to a thickness of 25–30 μm. The sample chamber was loaded with Ne as quasi-hydrostatic pressure transmitting medium using the gas loading system installed at BGI (Kurnosov et al., 2008). We used a piston-cylinder type DAC with BX90 and BX90-mini configuration (Kantor et al., 2012) equipped with tungsten carbide seats and Boehler-Almax anvil design (Boehler & De Hantsetters, 2007). Diamonds with culet sizes of 250 μm (runs SD005 and SD009) and 120 μm (run SD008) were used for IXS and XRD experiments. The complete list of experimental runs is provided in the supplementary information (Table S1 in Supporting Information S1).

2.3. IXS Measurements at SPring-8

IXS data were collected at BL35XU (Baron et al., 2000) at the SPring-8 synchrotron facility, Japan. We selected a ∼60 × 50 μm² piece of alloy with ∼5–10 μm thickness to obtain a reasonable signal intensity. During IXS data collection (runs SD005 and SD009) the DAC was set on the Eulerian cradle of the IXS spectrometer in a helium gas atmosphere. The beam size was focused to about 14 μm vertically and 17 μm horizontally (full-width at half maximum, FWHM) using a Kirkpatrick-Baez mirror pair (Ishikawa et al., 2013). A Si (999) instrument configuration was used providing 2.8 meV FWHM resolution at 17.794 keV. The scattered X-rays were collected by 12 crystals arranged in a two-dimensional array. The momentum transfer $Q = 2\,k_0 \sin(2\theta/2)$, which is defined as a function of the wave vector of the incident photons k_0 and the scattering angle 2θ, was selected by rotating the spectrometer arm in the horizontal plane. IXS spectra were collected for ∼8–10 hr over a Q range of 4.24–7.62 nm⁻¹ and momentum resolution of 0.40 nm⁻¹ full width at each experimental pressure. The sample was compressed offline to about 100 GPa at room temperature through steps of roughly 10 GPa according to Raman spectra measured at the center of the diamond culet (micro Raman spectroscopy system: 785 nm diode laser installed at BL10XU) (Akahama & Kawamura, 2006). The pressure was subsequently determined more accurately using the equation of state (EOS) of the sample determined by XRD.

The relationship between momentum transfer and energy of acoustic phonons was determined. The scattering produced by the longitudinal acoustic (LA) phonons was fit with a Lorentzian function to obtain the LA mode energy at each momentum transfer, Q. We then derived the aggregate compressional sound velocity V_P from a sine fit to the phonon dispersion using

$$E = 4.192 \times 10^{-4}\,V_P \times Q_{MAX} \times \sin\left(\frac{\pi}{2}\frac{Q}{Q_{MAX}}\right), \tag{1}$$

where E is the energy in meV, Q is the momentum transfer (nm⁻¹), V_P is the compressional wave sound velocity (km/s), and Q_{MAX} is the momentum transfer where the phonon dispersion turns over, roughly the boundary of the Brillouin zone. Details of the fitting procedure are given in the supplementary information.

2.4. Synchrotron Powder XRD Measurements

We determined the density of $Fe_{0.67}Ni_{0.06}Si_{0.27}$ alloy (runs SD005 and SD009) at the same pressures as IXS experiments by in situ XRD using a flat panel detector (C9732DK, Hamamatsu Photonics K.K.) calibrated using CeO_2 reference material. Diffraction still images were collected with acquisition times of 3 s at each pressure and then integrated using DIOPTAS software (Prescher & Prakapenka, 2015). The unit cell parameters, background and line-profile parameters of the sample were refined using JANA 2006 software (Petrícek, Dušek, & Palatinus, 2014).

The EOS of the same material (run SD008) was calculated from volume measurements up to 84.2(7) GPa using powder XRD. High-pressure XRD experiments were performed at P02.2 beamline, PETRA III, DESY in Hamburg, Germany (λ = 0.2915 Å) using a Perkin Elmer XRD1621 (2048 × 2048 pixels, 200 × 200 μm^2) flat panel detector and a beam size of 2(v) × 2(h) μm^2. In run SD008 we loaded a piece of Fe-Ni-Si alloy of ~20 × 15 μm^2 with ~5–10 μm thickness along with a piece of gold (pressure calibrant) in the sample chamber using Ne as a pressure medium. The sample-detector distance was calibrated using CeO_2. The pressure was manually increased by tightening the DAC screws in steps of ~5 GPa and evaluated using an equation of state for Au (Fei et al., 2007). 2D diffraction images were acquired for 5 s each. XRD data reduction (DIOPTAS program) and processing (JANA 2006) were used to obtain the lattice parameters. The P-V data of the alloy, obtained after Le Bail refinement, were fitted using EosFit7-GUI software (Angel et al., 2014; Gonzalez-Platas et al., 2016).

3. Results

3.1. XRD Results and Equation of State

Powder XRD measurements (runs SD005, SD008, SD009) reveal that $Fe_{0.67}Ni_{0.06}Si_{0.27}$ alloy is stable in the B2 structure (CsCl-type) throughout the entire investigated pressure range (6.8(2) – 98(3) GPa). An integrated diffraction pattern collected at 84.2(7) GPa and room temperature is shown in Figure S3 in Supporting Information S1. The Le Bail method was used for data processing to refine lattice parameters, peak shapes, and the background. The Debye rings of the sample (runs SD005 and SD009) collected at the IXS beamline BL35XU (beam size 17 × 14 μm^2) show a minor degree of inhomogeneous intensity distribution (Figure S4a in Supporting Information S1). Based on single crystal ultrasonic data the effect of preferred orientation on compressional sound velocities was estimated to be a maximum of ~10% (e.g., Liu et al., 2014), while molecular dynamics simulations studies (e.g., Belonoshko et al., 2007) indicate a degree of anisotropy of about 6% in V_P for *bcc* Fe at Earth's inner core conditions. These estimates are comparable to the magnitude of our uncertainties in compressional sound velocities for B2-$Fe_{0.67}Ni_{0.06}Si_{0.27}$ alloy and thus, we consider any effect of preferred orientation in V_P to be within the error bars (Section 3.2). On the other hand, 2D diffraction images collected at P02.2 DESY on run SD008 show spotted Debye rings at all pressures (Figure S4b in Supporting Information S1). We do not consider the main reason for these spots to be strongly preferred orientation, but rather the reduced beam size (2 × 2 μm^2) compared to powder crystallites (grain size estimated to be on the order of a few microns), and possibly poor grain sampling statistics of the polycrystalline sample. We, therefore, consider the preferred orientation in our sample to be minor.

The equation of state (EOS) collected in run SD008 is consistent with previous studies on Fe-Si based on observations of Edmund et al. (2020) that the addition of Ni does not affect compressibility (Figure S5 in Supporting Information S1). Observed differences between EOS parameters of this study and previous work (Kamada et al., 2018; Edmund, Antonangeli, Decremps, Morard, et al., 2019; Edmund, Antonangeli, Decremps, Miozzi, et al., 2019) are related to differences in composition and employed fitting models (third order Birch-Murnaghan (BM3) or Vinet). Volumes in the 10.4(1) – 84.2(7) GPa pressure range at 300 K were fitted to a second order Birch-Murnaghan (BM2) equation of state (K'_{T0} = 4) with the following coefficients: V_0 = 22.37(8) $Å^3$, K_{T0} = 222(6) GPa. To explore other possible models, we fitted data using a third order Birch Murnaghan and a Vinet equation of state. A comparison of the obtained statistical parameters showed that the addition of K'_{T0} did not improve the quality of the fit, which also appears more consistent with a BM2 EOS as seen in the F-f plot (Figure S6 in Supporting Information S1).

The complete list of refined lattice parameters is given in the supplementary material (Table S2 in Supporting Information S1) and was used to calculate the pressure and bulk modulus K_T from the measured volume for every pressure point of the IXS experiments as well as the shear wave velocities (V_S).
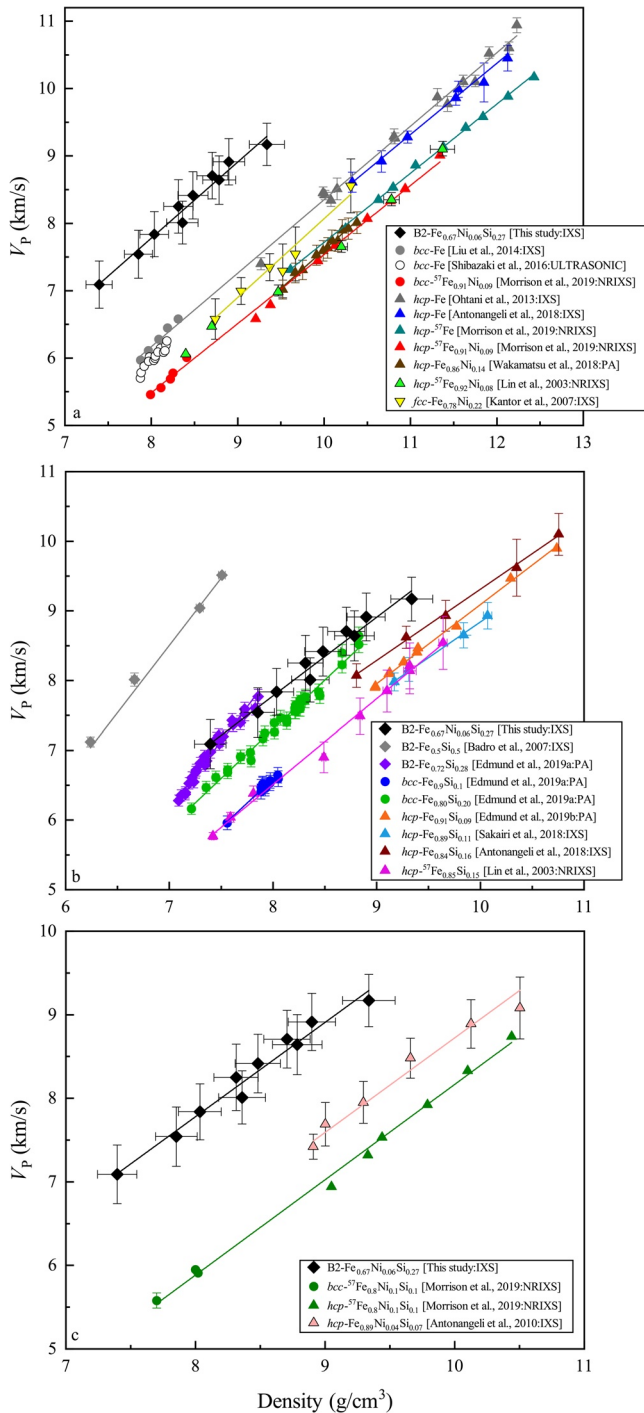
Figure 1. Birch's law of B2-$Fe_{0.67}Ni_{0.06}Si_{0.27}$ alloy compared with previous studies of pure Fe, Fe-Ni (a) Fe-Si (b), and Fe-Ni-Si alloys (c). Data reported by Lin et al. (2003) and Morrison et al. (2019) involve ^{57}Fe which is 1.8% denser than non-enriched Fe. Solid black lines show Birch's law fit our data in each panel. Crystal structure has a minimal effect since data with the same composition and different structures can be fitted with a common Birch's law (gray and red lines in Figure 1a, dark green line in Figure 1c). We included systematic errors in the estimation of error bars on the velocities (see supplementary information).

3.2. Sound Velocity and Birch's Law

IXS measurements (runs SD005 and SD009) were conducted at room temperature in the pressure range from 6.8(2) to 98(3) GPa. Figure S7 in Supporting Information S1 shows a fitted IXS spectrum collected at 98(3) GPa and momentum transfer 4.43 nm^{-1} on run SD009. The spectrum is characterized by an elastic peak, centered at zero energy, and inelastic features assigned to the longitudinal acoustic (LA) phonons of B2-$Fe_{0.67}Ni_{0.06}Si_{0.27}$ alloy and diamond and the transverse acoustic (TA) phonon of diamond. Experimental data and error bars are shown together with the best fit. Sample phonons are usually well resolved and visible for the investigated Q range (Figure S8 in Supporting Information S1). Energy positions of the phonons were determined by fitting data with Lorentzian functions and did not change within uncertainty if a pseudo-Voigt lineshape was used instead (Figure S9 in Supporting Information S1). The complete list of energy parameters and associated errors at different pressures and momentum transfers is given in Table S3 in Supporting Information S1. Results from each pressure were then fitted with a sinusoidal function to obtain the aggregate compressional sound velocity V_P (Equation 1). Dispersion curves of B2-$Fe_{0.67}Ni_{0.06}Si_{0.27}$ alloy for each pressure are shown in Figure S11 in Supporting Information S1. Energies are well fit at high Q but slightly overestimated at low Q, possibly due to stronger overlap of sample and diamond peaks at low Q. Deviations from fitted curves are largely within estimated uncertainties. The phonon energy of inelastic scattering increases with pressure; hence compressional sound velocity increases with pressure. The data obtained from fitting IXS spectra provide a good constraint on compressional sound velocity. The experimentally determined densities and velocities for the B2-$Fe_{0.67}Ni_{0.06}Si_{0.27}$ alloy are summarized in Table S4 in Supporting Information S1.

The measured compressional velocities V_P are plotted as a function of density in Figure 1 and compared with previous results for pure Fe, Fe-Ni, Fe-Si, and Fe-Ni-Si alloys with different crystal structures. The relation between V_P and density of B2-$Fe_{0.67}Ni_{0.06}Si_{0.27}$ alloy follows Birch's law,

$$V_P(km/s) = 1.13(7) \times \rho \; (g/cm^3) - 1.25(58), \qquad (2)$$

indicating a linear relationship between density and sound velocity.

Our velocity measurements for B2-$Fe_{0.67}Ni_{0.06}Si_{0.27}$ are systematically higher than for pure *bcc* Fe (Liu et al., 2014; Shibazaki et al., 2016) and *hcp* Fe (Antonangeli et al., 2018; Morrison et al., 2019; Ohtani et al., 2013) as a consequence of the effect of Si which increases V_P for a given density (Figure 1a). On the other hand, a comparison of elastic properties of pure Fe and Fe-Ni alloys (A. P. Kantor et al., 2007; Lin et al., 2003; Morrison et al., 2019; Wakamatsu et al., 2018) shows that Ni has the opposite effect to Si, reducing V_P at the same density with respect to pure Fe. We note that crystal structure has a minimal effect on the slope of Birch's law, as all data with the same composition can be fit to a common line (gray and red lines in Figure 1a, dark green line in Figure 1c). The difference observed between previous data of *hcp* Fe (Antonangeli et al., 2018; Ohtani et al., 2013) and *hcp* ^{57}Fe (Morrison et al., 2019) as well as between *hcp* Fe-Ni (A. P. Kantor et al., 2007; Wakamatsu et al., 2018) and *hcp* ^{57}Fe-Ni alloys (Lin et al., 2003; Morrison et al., 2019) is because ^{57}Fe is 1.8% denser than non-enriched iron.

Figure 1b shows our V_P-density measurements compared with previous studies conducted on Fe-Si alloys using IXS (Antonangeli et al., 2018; Badro

et al., 2007; Sakairi et al., 2018), NRIXS (Lin et al., 2003), and PA (Edmund, Antonangeli, Decremps, Morard, et al., 2019; Edmund, Antonangeli, Decremps, Miozzi, et al., 2019) techniques. All data show that increasing Si content increases V_P for a given density. There is some variation in the slope dV_P/dρ, which can be influenced by bonding (e.g., Edmund, Antonangeli, Decremps, Morard, et al., 2019), but can also be affected by experimental conditions (e.g., if a pressure medium was used or not) and different geometries used for different techniques (Edmund, Antonangeli, Decremps, Miozzi, et al., 2019). While differences in slope are relatively minor within the pressure range of data collection, they become more significant when data are extrapolated to core conditions.

Our data for B2-$Fe_{0.67}Ni_{0.06}Si_{0.27}$ are consistent with previous measurements of *bcc* and *hcp* Fe-Ni-Si alloys (Figure 1c). As above, Si and Ni have opposing effects on V_P at the same density. Overall, the compressional sound velocity of B2-$Fe_{0.67}Ni_{0.06}Si_{0.27}$ is dominated mainly by the effect of Si incorporation with a smaller effect due to Ni.

We derived the aggregate shear wave velocity V_S by combining our measurements of V_P and ρ with the adiabatic bulk modulus (K_S) from the EOS using the relation,

$$V_S = \left[\frac{3}{4} \left(V_P^2 - \frac{K_S}{\rho} \right) \right]^{\frac{1}{2}}. \tag{3}$$

Considering that the difference between K_S and the isothermal bulk modulus (K_T) is negligible at room temperature ($K_S = K_T (1 + \alpha\gamma T) \sim K_T$), we used K_T obtained from our isothermal EOS to calculate V_S. Results are shown in Table S4 in Supporting Information S1 together with uncertainties that were propagated on V_P, ρ and K_T.

4. Discussion

In order to compare our room temperature measurements with seismological models, we extrapolated the V_P-ρ and V_S-ρ linear relationships obtained from Birch's law to conditions of the inner core boundary (ICB) according to PREM (330 GPa and 6370 K, Alfè et al., 2002). Extrapolation of V_P for B2-$Fe_{0.67}Ni_{0.06}Si_{0.27}$ alloy was performed using a parameterization of Birch's law described by Sakamaki et al. (2016),

$$V_P(\rho, T) = M\rho + B + A(T - T_0)(\rho - \rho^*)], \tag{4}$$

where M and B are Birch's law coefficients at room temperature, and A and ρ^* are fixed parameters that describe the temperature dependence. Values of A and ρ^* were taken from Sakairi et al. (2018) and include the temperature dependence for Fe-Si alloys. We formulated the equation using $T_0 = 300$ K, $T = 6370$ K, $M = 1.13(7)$, $B = -1.25(58)$, $A = 3.8 \pm 1.8 \times 10^{-5}$ and $\rho^* = 15.4 \pm 1.5$ g/cm³. We estimated a large uncertainty for A to take the difference in composition into account between our B2-Fe-Ni-15 wt.% Si alloy and the Fe-6 wt.% Si alloy of Sakairi et al. (2018). We estimated the uncertainty of ρ^* to be of the same magnitude as that for *hcp*-Fe (Sakamaki et al., 2016). Error propagation of V_P was performed following Sakamaki et al. (2016). Extrapolation of the density to 330 GPa and 6370 K was performed using the isothermal EOS determined for the sample (Section 3.1) corrected for the thermal pressure (P_{th}). We applied the P_{th} correction using the Mie-Grüneisen Debye (MGD) model (e.g., Poirier, 2000). Thermoelastic parameters (i.e., Debye temperature θ, Grüneisen parameter γ and its logarithmic volume derivative q) of *hcp* and *hcp* + B2-$Fe_{0.84}Si_{0.16}$ (R. A. Fischer et al., 2014), *hcp*-$Fe_{0.81}Ni_{0.09}Si_{0.1}$ (Morrison et al., 2018), *hcp*-$Fe_{0.91}Si_{0.09}$ (Edmund, Antonangeli, Decremps, Miozzi, et al., 2019), and *hcp*-$Fe_{0.86}Ni_{0.05}Si_{0.9}$ (Edmund et al., 2020) from previous studies were used in the calculation. Table S5 in Supporting Information S1 summarizes the thermodynamic parameters used to extrapolate density and sound velocities to ICB conditions. Further details are given in supplementary text S2. V_S determination at ICB was performed by applying Equation 3 in which V_P was calculated using Equation 4, and ρ and K_S were obtained using the MGD model. Figure 2 shows that extrapolated data for *hcp*-Fe-Ni (triangles) and B2-$Fe_{0.67}Ni_{0.06}Si_{0.27}$ (colored diamonds) follow roughly a linear trend with PREM values for both V_P and V_S, motivating a more quantitative approach to determining properties of a mixture.

To test the hypothesis that the inner core is composed of a mixture of Si-depleted *hcp* and Si-enriched B2 phases, we used the linear mixing model presented by Badro et al. (2007) to determine the properties of an ideal mixture of *hcp* Fe-Ni and B2-$Fe_{0.67}Ni_{0.06}Si_{0.27}$. This arithmetic approach was also used by Wyllie et al. (1956) who calculated the average velocity of a two-phase mixture in porous media and is also frequently used to determine the
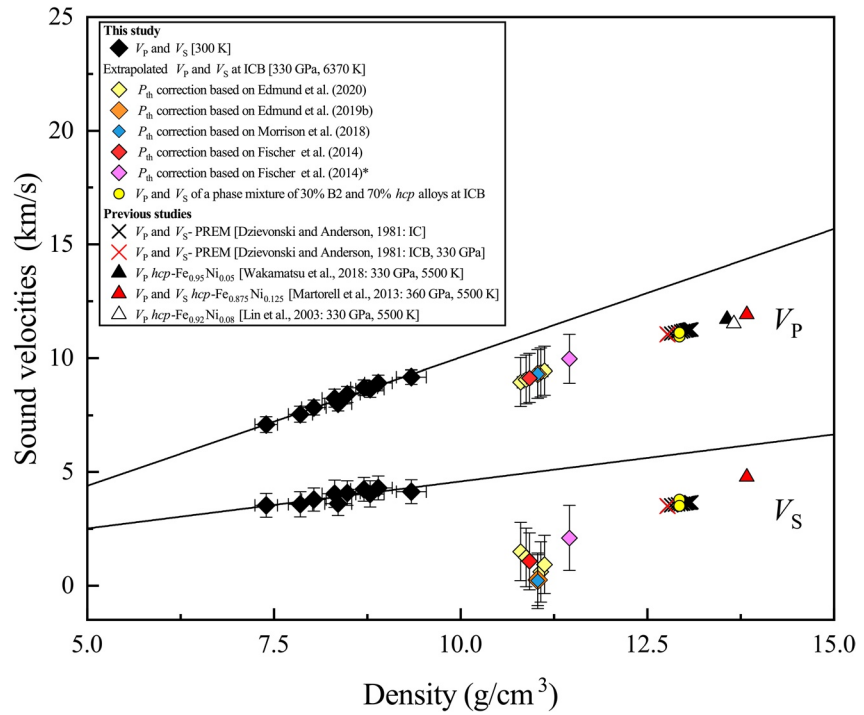
Figure 2. Density dependence of aggregate compressional (V_P) and shear (V_S) wave velocities of B2-Fe$_{0.67}$Ni$_{0.06}$Si$_{0.27}$ at inner core boundary conditions. Colored diamonds are the present data extrapolated to 330 GPa and 6370 K using different thermoelastic parameters for the thermal pressure correction P_{th} based on hcp-Fe$_{0.84}$Si$_{0.16}$: Fischer et al. (2014) (red); hcp + B2-Fe$_{0.84}$Si$_{0.16}$: Fischer et al. (2014) (magenta); hcp-Fe$_{0.81}$Ni$_{0.09}$Si$_{0.1}$: Morrison et al. (2018) (blue); hcp-Fe$_{0.91}$Si$_{0.09}$: Edmund, Antonangeli, Decremps, Miozzi, et al. (2019) (orange); hcp-Fe$_{0.86}$Ni$_{0.05}$Si$_{0.9}$: Edmund et al. (2020) (yellow) (from case #1 to case #4, see Table S5 in Supporting Information S1). Black diamonds and associated solid lines are Birch's law of B2-Fe$_{0.67}$Ni$_{0.06}$Si$_{0.27}$ at 300 K. Triangles represent V_P and V_S-density relations from previous selected studies of hcp Fe$_{0.92}$Ni$_{0.08}$ (white: Lin et al. (2003) at 330 GPa and 5500 K), hcp Fe$_{0.875}$Ni$_{0.125}$ (red: Martorell et al. (2013) at 360 GPa and 5500 K), hcp Fe$_{0.95}$Ni$_{0.05}$ and hcp Fe$_{0.86}$Ni$_{0.14}$ (black: Wakamatsu et al. (2018) at 330 GPa 5500 K). Yellow circles are estimated V_P and V_S averages of the mechanical mixture 30 vol. % B2 + 70 vol. % hcp consistent with preliminary reference Earth model (PREM) values within uncertainty. Crosses: PREM inner core (black); PREM values at inner core boundary (red).

velocity of rocks (e.g., Christensen & Salisbury, 1975). This model provides a good starting point since the dominant influence on density and sound velocity is Si composition. The average density ρ and sound velocity V_P of PREM can be expressed as (Badro et al., 2007):

$$\rho = x\rho^{FeNiSi} + (1 - x)\rho^{FeNi} \tag{5}$$

and,

$$V_P = \frac{V_P^{FeNiSi} V_P^{FeNi}}{\left[(1 - x)V_P^{FeNiSi} + x V_P^{FeNi}\right]}, \tag{6}$$

where x is the volume fraction of B2-Fe$_{0.67}$Ni$_{0.06}$Si$_{0.27}$ alloy, V_P^{FeNiSi} and V_P^{FeNi} are extrapolated compressional velocities at ICB of B2-Fe$_{0.67}$Ni$_{0.06}$Si$_{0.27}$ and Fe-Ni alloy (Wakamatsu et al., 2018), ρ^{FeNiSi} and ρ^{FeNi} are corresponding densities at ICB of B2-Fe$_{0.67}$Ni$_{0.06}$Si$_{0.27}$ and Fe-Ni alloy (Wakamatsu et al., 2018), and the P_{th} correction based on Fischer et al. (2014) was used. Solving Equations 5 and 6 simultaneously gives a volume fraction x of 0.30(5). Similar volume fractions are obtained within this uncertainty if velocities and densities of Fe-Ni alloy from Lin et al. (2003) or Martorell et al. (2013) are used instead. Similarly, volume fractions do not change outside of uncertainty if other temperatures within the inner core are used to solve Equations 5 and 6. To test the validity of our determination, we calculated elastic properties of the same composite assemblage (30 vol. % B2 + 70 vol. % hcp) at the ICB using the Voigt-Reuss-Hill (VRH) average (e.g., Man & Huang, 2011), which is commonly used to estimate elastic properties of polycrystalline materials. We derived bulk and shear moduli from V_P, V_S, and density of the B2 and hcp phases. Using the VRH approach, we obtained the same average elastic properties

within uncertainty as the linear mixing model by Badro et al. (2007). Estimated V_P and V_S averages of the mechanical mixture 30 vol. % B2 + 70 vol. % *hcp* are consistent with PREM values within uncertainty (yellow circles in Figure 2).

The inner core composition corresponding to the mixture 30 vol. % B2-$Fe_{0.67}Ni_{0.06}Si_{0.27}$ + 70 vol. % *hcp*-$Fe_{0.95}Ni_{0.05}$ is 3.9(5) wt.% Si. and 5.7(7) % Ni at ICB conditions. We consider the Si content to be well determined from this calculation due to the strong effect of Si on sound velocity, while Ni is less well constrained and depends on the Ni content of the Fe-Ni alloy endmember. We also determined Si and Ni content using *hcp* Fe-Ni data from Lin et al. (2003) and Martorell et al. (2013) at ICB conditions (i.e., 330 GPa and 6370 K) and found that, although the Si content is the same within uncertainty, the Ni content in the inner core varies as a function of the composition of the *hcp* endmember. For example, using *hcp*-$Fe_{0.875}Ni_{0.125}$ data from Martorell et al. (2013) and *hcp*-$Fe_{0.92}Ni_{0.08}$ data from Lin et al. (2003), the Ni content predicted in the inner core varies from ∼12(2) to ∼8(1) wt.%, respectively.

The estimated Si content, ∼3-5 wt.% agrees with values proposed by Sakairi et al. (2018) (3-6 wt.% Si), while it is slightly higher than the value proposed by Badro et al. (2007) (2.3 wt.% Si) and Antonangeli et al. (2010, 2018) (2 wt.% Si) and lower than the estimate of Z. Mao et al. (2012) (8 wt.% Si). The difference to the latter study might arise from the different models that they used to extrapolate V_P-ρ to the ICB (power law). The inferred amount of Ni (5-12 wt.%) is consistent with geochemical estimates (e.g., 5.2 wt.%, McDonough, 2003, 5-15 wt.% Ni, Li & Fei, 2014).

5. Conclusions

Sound velocity and density measurements performed on B2-$Fe_{0.67}Ni_{0.06}Si_{0.27}$ under pressure yielded values of V_P that are significantly faster than pure Fe at the same density, mainly as a consequence of the effect of Si on the elastic properties of pure Fe. We tested the hypothesis that the inner core is composed of a mixture of Si-depleted *hcp* and Si-enriched B2 phases, and found that PREM V_P and ρ values are consistent with an inner core consisting of a mixture of ∼30 vol % B2-$Fe_{0.67}Ni_{0.06}Si_{0.27}$ and ∼70 vol % *hcp* Fe-Ni, which corresponds to 3-5 wt.% Si and 5-12 wt.% Ni. We emphasize that the inferred amount of Si and Ni may vary depending on the presence of other light elements in the inner core (e.g., Caracas, 2017) and/or anharmonic/pre-melting effects of core material (Antonangeli et al., 2018; Martorell et al., 2013). Further uncertainties arise from the choice of thermoelastic parameters used for the temperature correction. The model could therefore be improved by performing sound velocity measurements on Fe-Ni-Si alloys at combined high pressure and high temperature.

Data Availability Statement

Data are available via the figshare repository: Figures: https://doi.org/10.6084/m9.figshare.13370795.v1. Tables: https://doi.org/10.6084/m9.figshare.13370792.v1.

References

Akahama, Y., & Kawamura, H. (2006). Pressure calibration of diamond anvil Raman gauge to 310 GPa. *Journal of Applied Physics*, *100*(4), 43516. https://doi.org/10.1063/1.2335683

Alfè, D., Gillan, M. J., & Price, G. D. (2002). Composition and temperature of the Earth's core constrained by combining ab initio calculations and seismic data. *Earth and Planetary Science Letters*, *195*(1–2), 91–98. https://doi.org/10.1016/S0012-821X(01)00568-4

Allègre, C. J., Poirier, J. P., Humler, E., & Hofmann, A. W. (1995). The chemical composition of the Earth. *Earth and Planetary Science Letters*, *134*(3–4), 515–526. https://doi.org/10.1016/0012-821X(95)00123-T

Angel, R. J., Gonzalez-Platas, J., & Alvaro, M. (2014). EosFit7c and a Fortran module (library) for equation of state calculations. *Zeitschrift Fur Kristallographie*, *229*(5), 405–419. https://doi.org/10.1515/zkri-2013-1711

Antonangeli, D., Morard, G., Paolasini, L., Garbarino, G., Murphy, C. A., Edmund, E., et al. (2018). Sound velocities and density measurements of solid *hcp*-Fe and *hcp*-Fe–Si (9 wt.%) alloy at high pressure: Constraints on the Si abundance in the Earth's inner core. *Earth and Planetary Science Letters*, *482*, 446–453. https://doi.org/10.1016/j.epsl.2017.11.043

Antonangeli, D., Siebert, J., Badro, J., Farber, D. L., Fiquet, G., Morard, G., & Ryerson, F. J. (2010). Composition of the Earth's inner core from high-pressure sound velocity measurements in Fe-Ni-Si alloys. *Earth and Planetary Science Letters*, *295*(1–2), 292–296. https://doi.org/10.1016/j.epsl.2010.04.018

Asanuma, H., Ohtani, E., Sakai, T., Terasaki, H., Kamada, S., Hirao, N., et al. (2008). Phase relations of Fe-Si alloy up to core conditions: Implications for the Earth inner core. *Geophysical Research Letters*, *35*(12), 2–5. https://doi.org/10.1029/2008GL033863

Badro, J., Fiquet, G., Guyot, F., Gregoryanz, E., Occelli, F., Antonangeli, D., & d'Astuto, M. (2007). Effect of light elements on the sound velocities in solid iron: Implications for the composition of Earth's core. *Earth and Planetary Science Letters*, *254*(1–2), 233–238. https://doi.org/10.1016/j.epsl.2006.11.025

Balchan, A. S., & Cowan, G. R. (1966). Shock compression of two iron-silicon alloys to 2.7 megabars. *Journal of Geophysical Research*, *71*(14), 3577–3588. https://doi.org/10.1029/jz071i014p03577

Baron, A. Q. R., Tanaka, Y., Goto, S., Takeshita, K., Matsushita, T., & Ishikawa, T. (2000). An X-ray scattering beamline for studying dynamics. *Journal of Physics and Chemistry of Solids*, *61*(3), 461–465. https://doi.org/10.1016/S0022-3697(99)00337-6

Belonoshko, A. B., Skorodumova, N. V., Davis, S., Osiptsov, A. N., Rosengren, A., & Johansson, B. (2007). Origin of the low rigidity of the Earth's inner core. *Science*, *316*(5831), 1603–1605. https://doi.org/10.1126/science.1141374

Birch, F. (1952). Elasticity and constitution of the Earth's interior. *Journal of Geophysical Research*, *57*(2), 227–286. https://doi.org/10.1029/jz057i002p00227

Birch, F. (1964). Density and composition of mantle and core. *Journal of Geophysical Research*, *69*(20). https://doi.org/10.1029/jz069i020p04377

Boehler, R., & De Hantsetters, K. (2007). New anvil designs in diamond-cells. *High Pressure Research*, *24*(3), 391–396. https://doi.org/10.1080/08957950412331323924

Brown, J. M., & McQueen, R. G. (1986). Phase transitions, Grüneisen parameter, and elasticity for shocked iron between 77 GPa and 400 GPa. *Journal of Geophysical Research*, *91*(B7), 7485–7494. https://doi.org/10.1029/jb091ib07p07485

Caracas, R. (2017). The influence of carbon on the seismic properties of solid iron. *Geophysical Research Letters*, *44*, 128–134. https://doi.org/10.1002/2016GL071109

Caracas, R., & Wentzcovitch, R. (2004). Equation of state and elasticity of FeSi. *Geophysical Research Letters*, *31*, 20. https://doi.org/10.1029/2004GL020601

Christensen, N. I., & Salisbury, M. H. (1975). Structure and constitution of the lower oceanic crust. *Reviews of Geophysics*, *13*(1), 57–86. https://doi.org/10.1029/RG013i001p00057

Dewaele, A., Loubeyre, P., Occelli, F., Mezouar, M., Dorogokupets, P. I., & Torrent, M. (2006). Quasihydrostatic equation of state of iron above 2 Mbar. *Physical Review Letters*, *97*(21), 29–32. https://doi.org/10.1103/PhysRevLett.97.215504

Dobson, D. P., Crichton, W. A., Bouvier, P., Vočadlo, L., & Wood, I. G. (2003). The equation of state of CsCl-structured FeSi to 40 GPa: Implications for silicon in the Earth's core. *Geophysical Research Letters*, *30*(1), 141–144. https://doi.org/10.1029/2002gl016228

Dobson, D. P., Vočadlo, L., & Wood, G. I. G. (2002). A new high-pressure phase of FeSi. *American Mineralogist*, *87*(5–6), 784–787. https://doi.org/10.2138/am-2002-5-623

Dziewonski, A. M., & Anderson, D. L. (1981). Preliminary reference Earth model. *Physics of the Earth Planetary Interiors*, *25*, 297–356. https://doi.org/10.1016/0031-9201(81)90046-7

Edmund, E., Antonangeli, D., Decremps, F., Miozzi, F., Morard, G., Boulard, E., et al. (2019). Velocity-density systematics of Fe-5wt%Si: Constraints on Si content in the Earth's inner core. *Journal of Geophysical Research: Solid Earth*, *124*(4), 3436–3447. https://doi.org/10.1029/2018JB016904

Edmund, E., Antonangeli, D., Decremps, F., Morard, G., Ayrinhac, S., Gauthier, M., et al. (2019). Structure and elasticity of cubic Fe-Si alloys at high pressures. *Physical Review B*, *100*(13), 134105. https://doi.org/10.1103/PhysRevB.100.134105

Edmund, E., Miozzi, F., Morard, G., Boulard, E., Clark, A., Decremps, F., et al. (2020). Axial compressibility and thermal equation of state of hcp Fe–5wt%Ni–5wt%Si. *Minerals*, *10*(2), 1–12. https://doi.org/10.3390/min10020098

Fei, Y., Murphy, C., Shibazaki, Y., Shahar, A., & Huang, H. (2016). Thermal equation of state of hcp-iron: Constraint on the density deficit of Earth's solid inner core. *Geophysical Research Letters*, *43*(13), 6837–6843. https://doi.org/10.1002/2016GL069456

Fei, Y., Ricolleau, A., Frank, M., Mibe, K., Shen, G., & Prakapenka, V. (2007). High-Pressure Geoscience Special Feature: Toward an internally consistent pressure scale. *Proceedings of the National Academy of Sciences*, *104*(22), 9182–9186. https://doi.org/10.1073/pnas.0609013104

Fischer, R. A., & Campbell, A. J. (2015). The axial ratio of hcp Fe and Fe-Ni-Si alloys to the conditions of Earth's inner core. *American Mineralogist*, *100*(11–12), 2718–2724. https://doi.org/10.2138/am-2015-5191

Fischer, R. A., Campbell, A. J., Caracas, R., Reaman, D. M., Dera, P., & Prakapenka, V. B. (2012). Equation of state and phase diagram of Fe-16Si alloy as a candidate component of Earth's core. *Earth and Planetary Science Letters*, *357*(358), 268–276. https://doi.org/10.1016/j.epsl.2012.09.022

Fischer, R. A., Campbell, A. J., Caracas, R., Reaman, D. M., Heinz, D. L., Dera, P., & Prakapenka, V. B. (2014). Equations of state in the Fe-FeSi system at high pressures and temperatures. *Journal of Geophysical Research: Solid Earth*, *119*, 3678–3699. https://doi.org/10.1002/2013JB010898

Fischer, R. A., Campbell, A. J., Reaman, D. M., Miller, N. A., Heinz, D. L., Dera, P., & Prakapenka, V. B. (2013). Phase relations in the Fe-FeSi system at high pressures and temperatures. *Earth and Planetary Science Letters*, *373*, 54–64. https://doi.org/10.1016/j.epsl.2013.04.035

Fischer, R. A., Nakajima, Y., Campbell, A. J., Frost, D. J., Harries, D., Langenhorst, F., et al. (2015). High pressure metal-silicate partitioning of Ni, Co, V, Cr, Si, and O. *Geochimica et Cosmochimica Acta*, *167*, 177–194. https://doi.org/10.1016/j.gca.2015.06.026

Gonzalez-Platas, J., Alvaro, M., Nestola, F., & Angel, R. (2016). EosFit7-GUI: A new graphical user interface for equation of state calculations, analyses and teaching. *Journal of Applied Crystallography*, *49*(4), 1377–1382. https://doi.org/10.1107/S1600576716008050

Hirao, N., Ohtani, E., Kondo, T., & Kikegawa, T. (2004). Equation of state of iron–silicon alloys to megabar pressure. *Physics and Chemistry of Minerals*, *31*, 329–336. https://doi.org/10.1007/s00269-004-0387-x

Ikuta, D., Ohtani, E., & Hirao, N. (2021). Two-phase mixture of Fe-Ni-Si alloys in the Earth's inner core. *Communications Earth and Environment*, *2*, 225. https://doi.org/10.1038/s43247-021-00298-1

Ishikawa, D., Uchiyama, H., Tsutsui, S., Fukui, H., & Baron, A. Q. R. (2013). Compound focusing for hard-x-ray inelastic scattering. *Advances in X-Ray/EUV Optics and Components*, *VIII 8848*, 88480F. https://doi.org/10.1117/12.2023795

Kamada, S., Suzuki, N., Maeda, F., Hirao, N., Hamada, M., Ohtani, E., et al. (2018). Electronic properties and compressional behavior of Fe-Si alloys at high pressure. *American Mineralogist*, *103*, 1959–1965. https://doi.org/10.2138/am-2018-6425

Kantor, A. P., Kantor, I. Y., Kurnosov, A. V., Kuznetsov, A. Y., Dubrovinskaia, N. A., Krisch, M., et al. (2007). Sound wave velocities of fcc Fe-Ni alloy at high pressure and temperature by mean of inelastic X-ray scattering. *Physics of the Earth and Planetary Interiors*, *164*(1–2), 83–89. https://doi.org/10.1016/j.pepi.2007.06.006

Kantor, I., Prakapenka, V., Kantor, A., Dera, P., Kurnosov, A., Sinogeikin, S., et al. (2012). BX90: A new diamond anvil cell design for X-ray diffraction and optical measurements. *Review of Scientific Instruments*, *83*(12), 125102. https://doi.org/10.1063/1.4768541

Kurnosov, A., Kantor, I., Boffa Ballaran, T., Lindhardt, S., Dubrovinsky, L., Kuznetsov, A., & Zehnder, B. H. (2008). A novel gas-loading system for mechanically closing of various types of diamond anvil cells. *Review of Scientific Instruments*, *79*(4), 045110. https://doi.org/10.1063/1.2902506

Kuwayama, Y., Sawai, T., Hirose, K., Sata, N., & Ohishi, Y. (2009). Phase relations of iron–silicon alloys at high pressure and high temperature. *Physics and Chemistry of Minerals*, *36*(9), 511–518. https://doi.org/10.1007/s00269-009-0296-0

Li, J., & Fei, Y. (2014). Experimental constraints on core composition. In *Treatise on Geochemistry* (2nd ed., p. 3). https://doi.org/10.1016/B978-0-08-095975-7.00214-X

Lin, J. F., Scott, H. P., Fischer, R. A., Chang, Y. Y., Kantor, I., & Prakapenka, V. B. (2009). Phase relations of Fe-Si alloy in Earth's core. *Geophysical Research Letters*, *36*(6). https://doi.org/10.1029/2008GL036990

Lin, J. F., Struzhkin, V. V., Sturhahn, W., Huang, E., Zhao, J., Hu, M. Y., et al. (2003). Sound velocities of iron-nickel and iron-silicon alloys at high pressures. *Geophysical Research Letters*, *30*(21), 1–4. https://doi.org/10.1029/2003GL018405

Liu, J., Lin, J. F., Alatas, A., & Bi, W. (2014). Sound velocities of bcc-Fe and $Fe_{0.85}Si_{0.15}$ alloy at high pressure and temperature. *Physics of the Earth and Planetary Interiors*, *233*, 24–32. https://doi.org/10.1016/j.pepi.2014.05.008

Lord, O. T., Walter, M. J., Dobson, D. P., Armstrong, L., Clark, S. M., & Kleppe, A. (2010). The FeSi phase diagram to 150 GPa. *Journal of Geophysical Research*, *115*(B6). https://doi.org/10.1029/2009JB006528

Man, C. S., & Huang, M. (2011). A simple explicit formula for the Voigt-Reuss-Hill average of elastic polycrystals with arbitrary crystal and texture symmetries. *Journal of Elasticity*, *105*(1), 29–48. https://doi.org/10.1007/s10659-011-9312-y

Mao, H. K., Kao, C., & Hemley, R. J. (2001). Inelastic x-ray scattering at ultrahigh pressures. *Journal of Physics: Condensed Matter*, *13*(34), 7847–7858. https://doi.org/10.1088/0953-8984/13/34/323

Mao, H. K., Wu, Y., Chen, L. C., Shu, J. F., & Jephcoat, A. P. (1990). Static compression of iron to 300 GPa and Fe0.8Ni0.2 alloy to 260 GPa: Implications for composition of the core. *Journal of Geophysical Research*, *95*(B13), 21737–21742. https://doi.org/10.1029/jb095ib13p21737

Mao, Z., Lin, J. F., Liu, J., Alatas, A., Gao, L., Zhao, J., & Mao, H. K. (2012). Sound velocities of Fe and Fe-Si alloy in the Earth's core. *Proceedings of the National Academy of Sciences of the United States of America*, *109*(26), 10239–10244. https://doi.org/10.1073/pnas.1207086109

Martorell, B., Vočadlo, L., Brodholt, J., & Wood, I. G. (2013). Strong premelting effect in the elastic properties of hcp-Fe under inner-core conditions. *Science*, *342*(6157). https://doi.org/10.1126/science.1243651

McDonough, W. F. (2003). Compositional model for the Earth's core. https://doi.org/10.1016/B0-08-043751-6/02015-6

McDonough, W. F., & Sun, S. S. (1995). The composition of the Earth. *Chemical Geology*, *120*(3–4), 223–253. https://doi.org/10.1016/0009-2541(94)00140-4

Morrison, R. A., Jackson, J. M., Sturhahn, W., Zhang, D., & Greenberg, E. (2018). Equations of state and anisotropy of Fe-Ni-Si alloys. *Journal of Geophysical Research: Solid Earth*, *123*(6), 4647–4675. https://doi.org/10.1029/2017JB015343

Morrison, R. A., Jackson, J. M., Sturhahn, W., Zhao, J., & Toellner, T. S. (2019). High pressure thermoelasticity and sound velocities of Fe-Ni-Si alloys. *Physics of the Earth and Planetary Interiors*, *294*, 106268. https://doi.org/10.1016/j.pepi.2019.05.011

Ohtani, E., Shibazaki, Y., Sakai, T., Mibe, K., Fukui, H., Kamada, S., et al. (2013). Sound velocity of hexagonal close-packed iron up to core pressures. *Geophysical Research Letters*, *40*(19), 5089–5094. https://doi.org/10.1002/grl.50992

Petrícek, V., Dušek, M., & Palatinus, L. (2014). Crystallographic computing system JANA2006: General features. *Zeitschrift für Kristallographie - Crystalline Materials*, *229*(5), 345–352. https://doi.org/10.1515/zkri-2014-1737

Poirier, J. P. (2000). *Introduction to the physics of the Earth's Interior*. Cambridge University Press. https://doi.org/10.1017/CBO9781139164467

Prescher, C., & Prakapenka, V. B. (2015). Dioptas: A program for reduction of two-dimensional X-ray diffraction data and data exploration. *High Pressure Research*, *35*(3), 223–230. https://doi.org/10.1080/08957959.2015.1059835

Ringwood, A. E. (1959). On the chemical evolution and densities of the planets. *Geochimica et Cosmochimica Acta*, *15*(4), 257–283. https://doi.org/10.1016/0016-7037(59)90062-6

Rubie, D. C. (1999). Characterizing the sample environment in multianvil high-pressure experiments. *Phase Transitions*, *68*(3), 431–451. https://doi.org/10.1080/01411599908224526

Rubie, D. C., Frost, D. J., Mann, U., Asahara, Y., Nimmo, F., Tsuno, K., et al. (2011). Heterogeneous accretion, composition and core-mantle differentiation of the Earth. *Earth and Planetary Science Letters*, *301*(1–2), 31–42. https://doi.org/10.1016/j.epsl.2010.11.030

Sakai, T., Ohtani, E., Hirao, N., & Ohishi, Y. (2011). Stability field of the hcp-structure for Fe, Fe-Ni, and Fe-Ni-Si alloys up to 3 Mbar. *Geophysical Research Letters*, *38*(9). https://doi.org/10.1029/2011GL047178

Sakairi, T., Sakamaki, T., Ohtani, E., Fukui, H., Kamada, S., Tsutsui, S., et al. (2018). Sound velocity measurements of hcp Fe-Si alloy at high pressure and high temperature by inelastic X-ray scattering. *American Mineralogist*, *103*(1), 85–90. https://doi.org/10.2138/am-2018-6072

Sakamaki, T., Ohtani, E., Fukui, H., Kamada, S., Takahashi, S., Sakairi, T., et al. (2016). Constraints on Earth's inner core composition inferred from measurements of the sound velocity of hcp-iron in extreme conditions. *Science Advances*, *2*(2). https://doi.org/10.1126/sciadv.1500802

Shibazaki, Y., Nishida, K., Higo, Y., Igarashi, M., Tahara, M., Sakamaki, T., et al. (2016). Compressional and shear wave velocities for polycrystalline bcc-Fe up to 6.3 GPa and 800 K. *American Mineralogist*, *101*(5), 1150–1160. https://doi.org/10.2138/am-2016-5545

Shibazaki, Y., Ohtani, E., Fukui, H., Sakai, T., Kamada, S., Ishikawa, D., et al. (2012). Sound velocity measurements in dhcp-FeH up to 70 GPa with inelastic X-ray scattering: Implications for the composition of the Earth's core. *Earth and Planetary Science Letters*, *313–314*(1), 79–85. https://doi.org/10.1016/j.epsl.2011.11.002

Siebert, J., Badro, J., Antonangeli, D., & Ryerson, F. J. (2013). Terrestrial accretion under oxidizing conditions. *Science*, *339*(6124), 1194–1198. https://doi.org/10.1126/science.1227923

Tateno, S., Kuwayama, Y., Hirose, K., & Ohishi, Y. (2015). The structure of Fe-Si alloy in Earth's inner core. *Earth and Planetary Science Letters*, *418*, 11–19. https://doi.org/10.1016/j.epsl.2015.02.008

Vočadlo, L., Price, G. D., & Wood, I. G. (1999). Crystal structure, compressibility and possible phase transitions in ε-FeSi studied by first-principles pseudopotential calculations. *Acta Crystallographica Section B: Structural Science*, *55*(4), 484–493. https://doi.org/10.1107/S0108768199001214

Wade, J., & Wood, B. J. (2005). Core formation and the oxidation state of the Earth. *Earth and Planetary Science Letters*, *236*(1–2), 78–95. https://doi.org/10.1016/j.epsl.2005.05.017

Wakamatsu, T., Ohta, K., Yagi, T., Hirose, K., & Ohishi, Y. (2018). Measurements of sound velocity in iron–nickel alloys by femtosecond laser pulses in a diamond anvil cell. *Physics and Chemistry of Minerals*, *45*(6), 589–595. https://doi.org/10.1007/s00269-018-0944-3

Wasson, J. T., & Chou, C. (1974). Fractionation of moderately volatile elements in ordinary chondrites. *Meteoritics and Planetary Science*, *9*(1), 69–84. https://doi.org/10.1111/j.1945-5100.1974.tb00063.x

Wyllie, M. R. J., Gregory, A. R., & Gardner, L. W. (1956). Elastic wave velocities in heterogeneous and porous media. *Geophysics*, *21*(1), 41–70. https://doi.org/10.1190/1.1438217

Zhang, J., & Guyot, F. (1999a). Experimental study of the bcc-fcc phase transformations in the Fe-rich system Fe-Si at high pressures. *Physics and Chemistry of Minerals*, *26*(6), 419–424. https://doi.org/10.1007/s002690050203

Zhang, J., & Guyot, F. (1999b). Thermal equation of state of iron and $Fe_{0.91}Si_{0.09}$. *Physics and Chemistry of Minerals*, *26*(3), 206–211. https://doi.org/10.1007/s002690050178